Chapter 7
Multi-objective Design Optimization Using High-Order Statistics for CFD Applications

Pietro M. Congedo, Gianluca Geraci, Remi Abgrall and Gianluca Iaccarino

Abstract This work illustrates a practical and efficient method for performing multi-objective optimization using high-order statistics. It is based on a Polynomial Chaos framework, and evolutionary algorithms. In particular, the interest of considering high-order statistics for reducing the number of uncertainties is studied. The feasibility of the proposed method is proved on a Computational Fluid-Dynamics (CFD) real-case application.

Keywords High-order statistics · Dimension reduction · Genetic algorithms · Robust optimization

7.1 Introduction

Optimization and design in the presence of uncertain operating conditions, material properties and manufacturing tolerances poses a tremendous challenge to the scientific computing community. In many industry-relevant situations the performance metrics depend in a complex, non-linear fashion on those factors and the construction of an accurate representation of this relationship is difficult. Probabilistic uncertainty quantification (UQ)approaches represent the inputs as random

P.M. Congedo (✉) · G. Geraci
INRIA Bordeaux Sud-Ouest, 200 Avenue de la Vieille Tour, 33405 Talence, France
e-mail: pietro.congedo@inria.fr

G. Geraci
e-mail: gianluca.geraci@inria.fr

R. Abgrall
Institut für Mathematik, Universität Zürich, Winterthurerstrasse 190 CH-8057, Zürich, Switzerland
e-mail: remi.abgrall@math.uzh.ch

G. Iaccarino
Mechanical Engineering Department, Bld 500, Stanford, CA 94305-3035, USA
e-mail: jops@stanford.edu

D. Greiner et al. (eds.), *Advances in Evolutionary and Deterministic Methods for Design, Optimization and Control in Engineering and Sciences*, Computational Methods in Applied Sciences 36, DOI 10.1007/978-3-319-11541-2_7

variables and seek to construct a statistical characterization of few quantities of interest. Several methodologies are proposed to tackle this problem; polynomial chaos (PC) methods [1] can provide considerable speed-up in computational time when compared to MC. In realistic situations however, the presence of a large number of uncertain inputs leads to an exponential increase of the cost thus making these methodologies unfeasible [2]. This situation becomes even more challenging when robust design optimization is tackled [3]. Robust optimization processes may require a prohibitive computational cost when dealing with a large number of uncertainties and a highly non-linear fitness function. Efforts in the development of numerical method are directed mainly to reduce the number of deterministic evaluations necessary for solving the optimization problem and for the uncertainty quantification (UQ) of the performances of interest. The overall cost is typically the product of the cost of the two approaches because the stochastic analysis and the optimization strategy are completely decoupled. Decoupled approaches are simple but more expensive than necessary.

Several UQ methods have been developed with the objective of reducing the number of solution required to obtain a statistical characterization of the quantity of interest. An alternative solution is based on approaches attempting to identify the relative importance of the input uncertainties on the output. A well known methodology is based on a decomposition of the variance of the quantity of interest in contributions closely connected to each of the input uncertainties (main effects) or combined inputs [4]. Recently, a practical way to decompose high-order statistical moments has been also proposed [5].

In this work, we illustrate an efficient multi-objective optimization method taking into account high-order statistic moments, such as the third and fourth-order statistic moments, i.e. skewness and kurtosis, respectively. These moments can be easily computed by means of a Polynomial Chaos (PC) method. A simplified test-case is presented that displays the importance of considering high-order moments during the optimization. The efficiency of the method in terms of computational cost and fitness function complexity is verified in a realistic CFD-case optimization problem.

7.2 Computing High-Order Statistics by Using Polynomial Chaos Techniques

This section is devoted to show how formulas of variance, skewness and kurtosis can be obtained using a polynomial chaos framework (for more details see Ref. [5]). If a polynomial chaos formulation is used, an approximation $\tilde{f}$ of the function f is provided

$$f(\boldsymbol{\xi}) \approx \tilde{f}(\boldsymbol{\xi}) = \sum_{k=0}^{P} \beta_k \Psi_k(\boldsymbol{\xi}), \tag{7.1}$$

where P is computed according to the order of the polynomial expansion n_0 and the stochastic dimension of the problem d

$$P + 1 = \frac{(n_0 + d)!}{n_0! d!}. \tag{7.2}$$

Each polynomial $\Psi_k(\boldsymbol{\xi})$ of total degree n_o is a multivariate polynomial form which involve tensorization of 1D polynomial form by using a multi-index $\boldsymbol{\alpha}^k \in \mathbb{R}^d$, with $\sum_{i=1}^{d} \boldsymbol{\alpha}_i^k \leq n_0$:

$$\Psi_k(\boldsymbol{\xi} \cdot \boldsymbol{m}^{\star,k}) = \prod_{\substack{i=1 \\ m_i^{\star,k} \neq 0}}^{d} \psi_{\alpha_i^k}(\xi_i) \tag{7.3}$$

where the multi index $\boldsymbol{m}^{\star,k} = \boldsymbol{m}^{\star,k}(\boldsymbol{\alpha}^k) \in \mathbb{R}^d$ is a function of $\boldsymbol{\alpha}^k$: $\boldsymbol{m}^{\star,k} = (m_1^{\star,k}, \ldots, m_d^{\star,k})$, with $m_i^{\star,k} = \alpha_i^k / \left|\left|\alpha_i^k\right|\right|_{\neq 0}$.

Remark that, for each polynomial basis, $\psi_0(\xi_i) = 1$ and then $\Psi_0(\boldsymbol{\xi}) = 1$. Then, the first coefficient β_0 is equal to the expected value of the function, i.e. $E(f)$. The polynomial basis is chosen accordingly to the Wiener-Askey scheme in order to select orthogonal polynomials with respect to the probability density function $p(\boldsymbol{\xi})$ of the input. Thanks to the orthogonality, the following relation holds

$$\int_{\Xi} \Psi_i(\boldsymbol{\xi}) \Psi_k(\boldsymbol{\xi}) p(\boldsymbol{\xi}) \mathrm{d}\xi = \delta_{ij} \langle \Psi_i(\boldsymbol{\xi}), \Psi_i(\boldsymbol{\xi}) \rangle \tag{7.4}$$

where $\langle \cdot, \cdot \rangle$ indicates the inner product and δ_{ij} is the Kronecker delta function.

The orthogonality can be advantageously used to compute the coefficients of the expansion in a non-intrusive PC framework

$$\beta_k = \frac{\langle f(\boldsymbol{\xi}), \Psi_k(\boldsymbol{\xi}) \rangle}{\langle \Psi_k(\boldsymbol{\xi}), \Psi_k(\boldsymbol{\xi}) \rangle}, \quad \forall k. \tag{7.5}$$

Note that the coefficients of the PC expansion are computed by a quadrature employing the points generated by a full tensorization of monodimensional quadrature rules. In particular, employing uniform distribution for the stochastic variables, a Legendre quadrature is chosen following the so-called Wiener-Askey scheme.

Variance (σ^2), skewness (s) and kurtosis (k) can be computed as follows:

$$\sigma^2 = E(f^2) - E(f)^2 = \sum_{k=1}^{P} \beta_k^2 \langle \Psi_k^2(\boldsymbol{\xi}) \rangle. \tag{7.6}$$

$$s = \sum_{k=1}^{P} \beta_k^3 \langle \Psi_k^3(\boldsymbol{\xi}) \rangle$$

$$+3\sum_{i=1}^{P}\beta_i^2\sum_{\substack{j=1\\j\neq i}}^{P}\beta_j\langle\Psi_i^2(\boldsymbol{\xi}),\Psi_j(\boldsymbol{\xi})\rangle$$
$$+6\sum_{i=1}^{P}\sum_{j=i+1}^{P}\sum_{k=j+1}^{P}\beta_i\beta_j\beta_k\langle\Psi_i(\boldsymbol{\xi}),\Psi_j(\boldsymbol{\xi})\Psi_k(\boldsymbol{\xi})\rangle, \tag{7.7}$$

$$k=\int f^4(\boldsymbol{\xi})p(\boldsymbol{\xi})\mathrm{d}\xi-4E(f)s-6\sigma^2E(f)^2-E(f)^4$$
$$=\sum_{k=1}^{P}\beta_k^4\langle\Psi_k^4(\boldsymbol{\xi})\rangle+4\sum_{i=1}^{P}\beta_i^3\sum_{\substack{j=1\\j\neq i}}^{P}\beta_j\langle\Psi_i^3,\Psi_j\rangle$$
$$+6\sum_{i=1}^{P}\beta_i^2\sum_{j=i+1}^{P}\beta_j^2\langle\Psi_i^2,\Psi_j^2\rangle$$
$$+12\sum_{i=1}^{P}\beta_i^2\sum_{\substack{j=1\\j\neq i}}^{P}\beta_j\sum_{\substack{k=j+1\\k\neq i}}^{P}\beta_k\langle\Psi_i^2,\Psi_j\Psi_k\rangle$$
$$+24\sum_{i=1}^{P}\sum_{j=i+1}^{P}\sum_{k=j+1}^{P}\sum_{h=k+1}^{P}\beta_i\beta_j\beta_k\beta_h\langle\Psi_i\Psi_j,\Psi_k\Psi_h\rangle. \tag{7.8}$$

7.3 Introducing More Sensitivity Indices

As introduced by Sobol [6], sensitivity indexes for variance can be computed for each conditional contribution as follows:

$$\sigma_{\boldsymbol{m_i}}^{2,\mathrm{SI}}=\frac{\sigma_{\boldsymbol{m_i}}^2}{\sigma^2}. \tag{7.9}$$

Here, we introduce new sensitivity indexes, basing on the decomposition of skewness and kurtosis, as follows

$$\begin{aligned}s_{\boldsymbol{m_i}}^{\mathrm{SI}}&=\frac{s_{\boldsymbol{m_i}}}{s}\\ k_{\boldsymbol{m_i}}^{\mathrm{SI}}&=\frac{k_{\boldsymbol{m_i}}}{k}.\end{aligned} \tag{7.10}$$

If a total sensitivity index is needed, i.e. it is necessary to compute the overall influence of a variable, it can be computed summing up all the contributions in which the variable is present

$$\begin{aligned} \mathrm{TSI}_j &= \sum_{\xi_j \in (\boldsymbol{\xi} \cdot \boldsymbol{m}_i)} \sigma^{2,\mathrm{SI}}_{\boldsymbol{m}_i} \\ \mathrm{TSI}^s_j &= \sum_{\xi_j \in (\boldsymbol{\xi} \cdot \boldsymbol{m}_i)} s^{\mathrm{SI}}_{\boldsymbol{m}_i} \\ \mathrm{TSI}^k_j &= \sum_{\xi_j \in (\boldsymbol{\xi} \cdot \boldsymbol{m}_i)} k^{\mathrm{SI}}_{\boldsymbol{m}_i}. \end{aligned} \tag{7.11}$$

7.3.1 Dimensional Reduction in the Truncation Sense

The first test case is represented by the following quadratic g-function:

$$f(\boldsymbol{\xi}) = \prod_{i=1}^{4} \frac{|4\xi_i - 2| + a_i}{1 + a_i} \tag{7.12}$$

where $\xi_i \sim \mathscr{U}(0, 1)$. Two possible choices of the coefficients are considered here

- $a_i = (i - 1)/2$ the so called linear g-function f_{glin}
- $a_i = i^2$ the so called quadratic g-function f_{gquad}.

From the analysis, it is possible to note that the third and fourth variables seem to be meaningless for the variance based indexes. Their total sensitivity indexes sum up to 0.05 for the variance, while exceed 0.15 for both skewness and kurtosis. Considering only the sensitivity indexes computed on the variance the decision-maker could be tempted to neglect the variables ξ_3 and ξ_4. In this case the ANOVA expansion will loose all the terms containing ξ_3 and ξ_4

$$\begin{aligned} f_{G1} &= f_0 + f_1(\xi_1) + f_2(\xi_2) + f_{12}(\xi_1, \xi_2) \\ f_{G2} &= f_0 + f_1(\xi_1) + f_2(\xi_2) + f_{12}(\xi_1, \xi_2) + f_3(\xi_3) + f_{13}(\xi_1, \xi_3) + f_{23}(\xi_2, \xi_3) + f_{123}(\xi_1, \xi_2, \xi_3), \end{aligned} \tag{7.13}$$

where in the first case f_{G1} both are neglected; while for f_{G2} only ξ_4 is neglected. In this case the ANOVA terms can be computed analytically and, from them, the statistics too. In the Table 7.1 the percentage errors, for the first four central moments, have been reported with respect the analytical exact solution for both the reduced models f_{G1} and f_{G2}.

Table 7.1 Percentage $\left(\frac{abs(\mu - \mu_{ex})}{\mu_{ex}} \times 100\right)$ errors related to the reduced g-function f_{G1} and f_{G2}

Function	Variance	Skewness	Kurtosis
f_{G1}	4.7997	29.236	15.039
f_{G2}	1.2369	7.7705	4.0632

The Table 7.1 makes evident as an error of only 5 % on the variance can correspond to a much greater error on the higher moments. The effect of a such behavior is clear looking at the Fig. 7.1 where the probability density function has been computed for both f_{G1} and f_{G2} and compared with the complete function (7.12). In this case the model with only the first two variables looses both the tails while a good approximation is achieved in the central part. However this test case clearly shows that considering only the sensitivity indexes based on the variance could be very dangerous if the reduced model need to be obtained for safety purpose. The information related to the less probable realizations of the system are totally lost and in this case the pdf resuls to be analytically bounded between the values of f equal to 0.4 and 1.8. If the third variable is included in the reduced model both variance and skewness are included with an error lower than 5 %, while the error on the skewness remains lower than 8 %. The total sensitivity indexes associated to the fourth variable is lower than 5 % for the three moments. The improvement of the model on the base of the inclusion of the third variable is evident in Fig. 7.1 where the pdf of the reduced model recover both the tails and better approximate the pdf of the complete function.

From a practical point-of-view the dimensional reduction of the model has commonly obtained freezing the neglected parameters. For an analytical function, as here of interest, it is possible to compute the constant values to choose, for both ξ_3 and ξ_4, to obtain a reduced model that preservers both the expectancy and the variance of the original complete model. Of course the two requirements cannot be satisfied contemporary but a set of values of constant satisfying the mean and the variance can be obtained analytically requiring (having a product tensorial function)

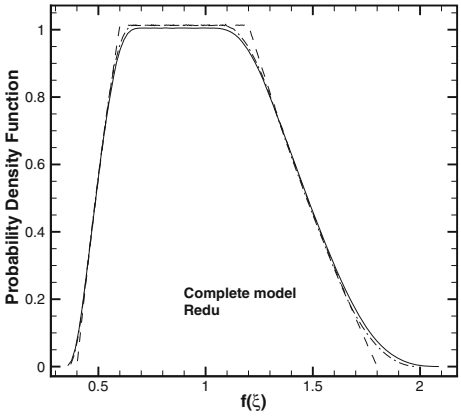

Fig. 7.1 PDFs for the complete g-function and the reduced models (see Eq. 7.13)

$$\frac{|4\bar{\xi_j} - 2| + a_j}{1 + a_j} = 1$$

$$\left(\frac{|4\bar{\xi_j} - 2| + a_j}{1 + a_j}\right)^2 = \int_0^1 \left(\frac{|4\xi_j - 2| + aj}{1 + a_j}\right)^2 \mathrm{d}\xi_j. \tag{7.14}$$

The following values can be analytically computed for the two variables: $\xi_3 = \{1/4, 3/4, 91/120, 29/120\}$ and $\xi_4 = \{1/4, 3/4, 77/102, 25/102\}$.

In the Fig. 7.2 the pdf relative to the complete quadratic g-function freezing the parameters ξ_3 and ξ_4 are reported compared to the complete pdf and the totally reduced one.

From Fig. 7.2 it is evident that freezing parameter to assure the correctness of the mean and the variance produces pdf very close to that one obtained neglecting entirely the ANOVA terms. From a practical point-of-view the analysis of the reduced model can be carried out both with the ANOVA reduced model (if it is analytically possible to compute integrals) of by freezing the parameter to neglect satisfying the requirement on the expectancy and variance. In both case the results make in evidence as the analysis on the variance based sensitivity indexes needs to be supplemented by information from sensitivity indexes of higher order to be confident that the reduction of the model can be realized without deteriorate too much the information carried by the reduced model in term of distribution of the realizations, especially in the tails.

In the second part of this section the function f_1 has been analyzed. For the third variable, the level of the TSI 1.55 %, has resulted to be less than the threshold of 2 %, indicated in [7], to detect meaningless parameters. A dimensional reduced model can be obtained freezing the third parameter, or equivalently for what shown in the first part of this section, neglecting all the ANOVA terms in which the variable ξ_3 is present

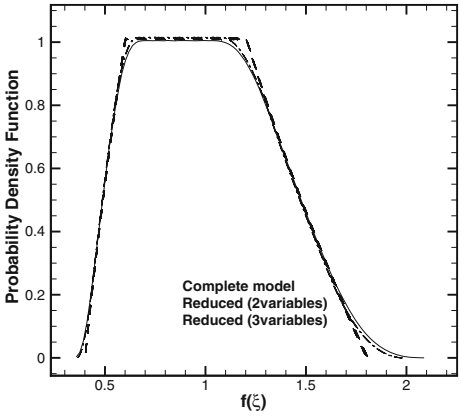

Fig. 7.2 PDFs for the complete g-function and the reduced models freezing the remaining parameters

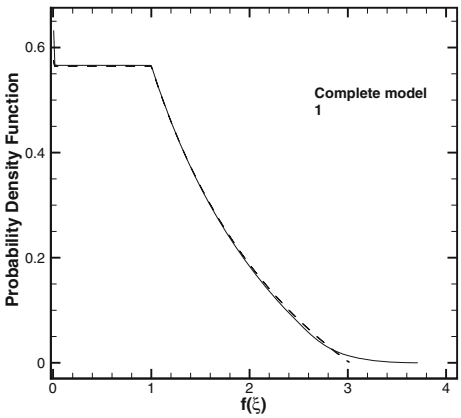

Fig. 7.3 PDFs for the complete f_1 and the reduced models freezing the third parameter

$$\hat{f}_1 = f_0 + f_1(\xi_1) + f_2(\xi_2) + f_{12}(\xi_1, \xi_2). \tag{7.15}$$

If the variable ξ_3 is chosen to recover the exact value of the mean and the variance of the complete model the following values are obtained: $\xi_3 = \{0.4282865945, 0.4166346546\}$. In the Fig. 7.3 the pdf for the complete model and the one freezing the third parameters have been reported. Even in this case, even with a model that it is able to obtain an error on the variance less than the 2 % (that for an engineering application can be very optimistic as goal for a metamodel) the information about the tails of the distributions are, again, totally lost. Of course the intent of this paper and of this section is not to criticize the use of the variance estimator, but to make evident that to obtain a metamodel to employ, for instance, for safety purpose the information relative to high-order sensitivity indexes should be considered. In all the case proposed and in many other, not reported here only for brevity, appear evident that only when even the high-order sensitivity indexes have reached a safety threshold (about 5 %) the model can be really (and more safely) truncated.

7.4 Multi-objective Design Optimization

7.4.1 Importance of Skewness in Decomposition

This paragraph is devoted to show how important is to control the skewness during an optimization process. Let us consider the following polynomial function:

$$f = a\,(xz + xy) + b\left(x^2 + z^2\right) + (cba)\,y^2 \tag{7.16}$$

where x, y and z vary between 0 and 1 with an uniform pdf. Parameters a, b and c are design parameters that vary between -5 and 5. For this function, it is possible

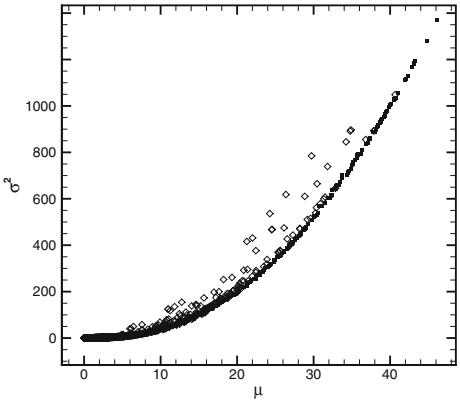

Fig. 7.4 Pareto front in the plan μ–σ^2 for the bi-objectives and three-objectives problem

to compute analytically high-order statistics, as functions of the design parameters. In order to show the importance to take into account also the high-order statistics in the robust optimization, different types of optimization are performed using several objective functions.

First, a classical bi-objective optimization is performed, where the mean of the function is maximized and its variance minimized. The Pareto front is reported in Fig. 7.4. No measures of skewness have been used during the optimization process, then the Pareto front is constituted by various designs displaying a very large variation of skewness.

Now, let us consider a three-objectives optimization, i.e. consisting in the maximization of the mean, the minimization of the variance and the minimization of the absolute value of the conditional skewness s_{xy}. In this case, the Pareto front is no more constituted by a curve, but by a surface in a 3D plan. The Pareto front is represented by means of 2D representation in the Figs. 7.4 and 7.5 with projections on the plans μ–σ^2, μ–s_{xy} and σ^2–s_{xy}, respectively. As shown in Fig. 7.5, designs belonging to the Pareto front display a large variation of the conditional skewness.

Now, let us compare the results obtained with both optimizations. In Fig. 7.4, we show Pareto fronts in the plan μ–σ^2. Designs obtained with the three-objectives optimization are dominated (with respect to only μ and σ^2) by the designs coming from the bi-objectives optimization. This is reasonable seeing that designs from bi-objective optimization are not influenced by the skewness s_{xy} during the optimization.

In Fig. 7.6, curves associated to the three-objectives optimization are obtained by the 3D Pareto front regarding only the designs having a skewness lower than 0.0001. Remark that individuals of this Pareto front take values of μ lower than 3.2 and values of σ^2 lower than 4.4. Moreover, they could be dominated in terms of μ and σ^2 by some individuals of the Pareto front obtained from the bi-objectives optimization.

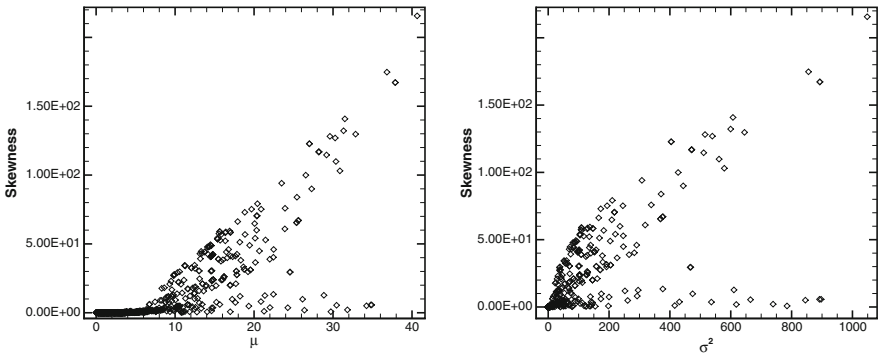

Fig. 7.5 Pareto front in the plan μ–s_{xy} (on the *left*) and σ^2–s_{xy} (on the *right*) for the three-objectives optimization

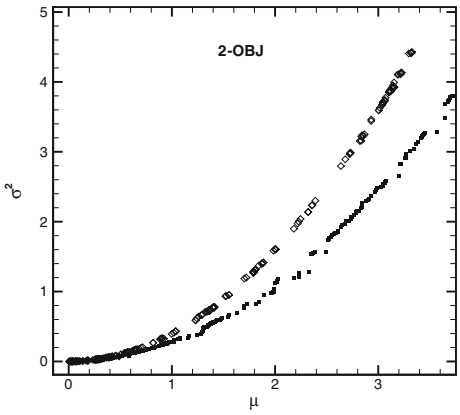

Fig. 7.6 Pareto front in the plan μ–σ^2 for the three-objectives optimization (extracted by the complete one considering only skewness inferior to 0.0001) and the bi-objective optimization

Here, the interest is to get a Pareto front that is not sensitive to large variation in the skewness, since designs obtained from bi-objective optimization could present large skewness values. This displays the great interest to estimate high-order statistics during optimization.

7.4.2 Description of the Algorithm

In this section, the algorithm for multi-objective robust design optimization is described. The strategy is constituted by two steps, that are schematically represented in Figs. 7.7 and 7.8. In the first step, (reported in the Fig. 7.7), a design of experience in the design variables space (called hereafter DOE), i.e. an initial set of design variables y, is generated. For each design variable y of the DOE, a high-order decomposition analysis is performed by computing for each uncertainty j, TSI_j and

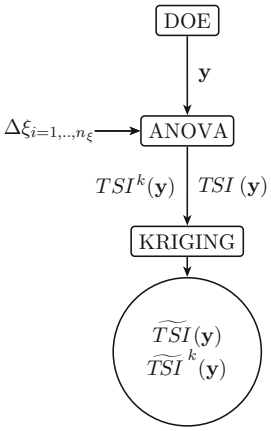

Fig. 7.7 Compact scheme for the kriging procedure

TSI_j^k. Then *TSI* is computed for each y of the DOE and for each uncertainty. A TSI response surface is built for each uncertainty and for each statistical moment as function of design variable space, i.e. $\widetilde{TSI}_j(y)$ and $\widetilde{TSI}_j(y)^k$, by means of a kriging method based on a DACE approach. The advantage of this methodology is the possibility of implement an adaptive response surface in order to minimize the statistical error between the real function and the extrapolated one.

In the second step (represented in Fig. 7.8), basing on the criterion for the *TSI*, the reduced stochastic problem is performed for each point of the DOE, where mean and variance are computed. Genetic algorithms are applied in order to compute new individuals basing on $\mu(y)$ and $\sigma(y)$. The NSGA algorithm [8] is used. The main tuning parameters of the algorithm are the population size, the number of generations, the crossover and mutation probabilities pc, pm and the so-called sharing parameter r used to take into account the relative isolation of an individual along a dominance front. Typical values for pc, pm are, respectively, 0.9 and 0.1; values of r are retained following a formula given in [8] that takes into account the population size and the number of objectives. Then, for the new design, mean and variance are computed for the reduced stochastic problem. Algorithm continues until convergence of genetic

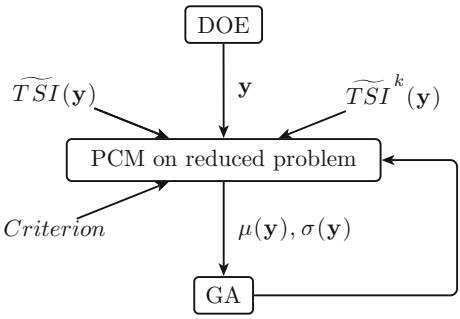

Fig. 7.8 Compact scheme for the overall optimization strategy

algorithms. For further validation of the algorithm, a complete stochastic analysis is performed for each optimal design in order to verify *TSI* for each uncertainty.

The criterion for *TSI* is based on a double verification on TSI_j and TSI_j^k. In particular, when the uncertainty j is considered, the criterion on TSI_j is applied (2 % based on Hestaven criterion) only if the ranking associated to j is the same for TSI_j and TSI_j^k.

7.4.3 Base Configuration and Sources of Uncertainty

In the present work, the turbine blade under consideration is the two dimensional VKI LS-59 cascade, a configuration which has been widely studied [9, 10]. An unstructured CFD dense-gas solver is used to ensure the reliability of the computed results for dense gas flows through a turbine cascade (for more details see Ref. [10]).The two-dimensional flow domain is discretized by a structured C-grid comprised of 192×16 cells. The boundary conditions are imposed as follows: at the inlet and outlet boundaries, non-reflecting boundaries are applied using the method of characteristics; a slip condition is imposed at the wall, which uses multi-dimensional linear extrapolation from interior points to calculate the wall pressure; periodicity conditions are prescribed at the inter-blade passage boundaries.

The siloxane *dodecamethylcyclohexasiloxane* ($C_{12}H_{36}Si_6O_6$), commercially known as D_6, is the fluid considered in this study. The physical properties of D_6 are reported in Table 7.2. The Peng-Robinson (PRSV) equation is used as thermodynamic model for D6. It depends on the following parameters, the fluid acentric factor ω, the isobaric specific heat in the ideal gas state, i.e. $c_{v\infty}$, and a fluid-dependent parameter n (the mean values of these parameters for D_6 are defined in Table 7.3).

Performance of the turbine cascade can be evaluated by using several output criteria. Here, the power output per unit depth (PO) expressed as $\Delta h \cdot \dot{m}/w_{mol}$ [W] is taken into account, where Δh is the enthalpy variation through turbine stage, $\dot{m}$ is the mass flow rate and w_{mol} is the molecular weight.

Three main sources of uncertainties are considered in this study (globally eight uncertainties): (i) the uncertainties on the operating conditions, i.e. inlet total temperature, T_{in}/T_c, inlet total pressure, p_{in}/p_c, angle of incidence β and the stagger angle θ, (ii) the uncertainties on the thermodynamic model, i.e. ω, $c_{v\infty}$ and n, and uncertainties on geometrical parameters, i.e. the blade thickness ϕ. Basing on [11], the 3.0 % of uncertainty for the temperature and pressure levels at the inlet conditions has

Table 7.2 Thermodynamic data for D_6, where M is the percentage molecular weight, and T_b is the boiling temperature at 1 atm

M (g/mole)	T_c (K)	P_c (kPa)	T_b (K)
444.9	645.8	961	518.1

Table 7.3 Thermodynamic constants for D6, PRSV equation of state, mean and min/max values for the uniform probability density function, data taken from [4]

	n	$c_{v\infty}$	ω
Mean	0.5729	105.86	0.7361
Range	0.5385–0.6073	99.50–112.20	0.7214–0.7508

been taken into account. The PRSV thermodynamic model is considered as a good trade-off between the accuracy of thermodynamic properties and the functional complexity since it depends on a limited number of parameters, hence a reduced number of uncertainty sources [11]. The following uncertainties are retained for this model (see the Table 7.3 and Ref. [11]), listed with their associated error bars: the acentric factor ω (2 %), the isobaric specific heat in the ideal gas state and a fluid-dependent parameter n (6 %). For the other parameters, it is assumed an uncertainty of 3 % for the angle of incidence β and the stagger angle θ, and an uncertainty of 2 % for the thickness ϕ.

7.4.4 Problem Definition

The objective is to find the optimal values for T_{in}/T_c, p_{in}/p_c, β and θ (four design variables) in order to maximize the mean of power output, $\mu(PO)$, and to minimize its standard deviation, $\sigma(PO)$ (two objective-optimization problem). Ranges for each design variable are defined in Table 7.4. Remark that the lower limit for the temperature is given by the saturation curve limit (SCL). Seeing that CFD code can compute only 1-phase flows, it has to be verified that the uncertainty region does not cross the maximal saturation curve (that can be computed as the upper limit of the 100 % confidence intervals when uncertainties on thermodynamic model are taken into account).

Finally, the optimization problem consists in finding the optimal values for four design variables where the output to maximize is dependent from eight uncertainties.

7.4.5 Optimization

A design of experiment (DOE) of 50 elements in the four design variable space is generated. Then, for each design, a quasi-Montecarlo plan (based on Sobol sequences) of two hundred individuals in the stochastic plan is generated and TSI is computed for

Table 7.4 Ranges of design variables in the optimization plan

p_{in}/p_c	T_{in}/T_c	β	θ
0.7–0.98	SCL–1.15	25°–35°	29°–39°

each uncertainty. The convergence of TSI indexes for each uncertainty and design is verified by increasing the number of individuals until five hundred. TSI for variance and kurtosis have been computed, displaying very small differences.

In Fig. 7.9, TSI (based on variance) contours are reported for each uncertainty in the plan p-T, where the point in the plan p-T is associated to the couple (p_{in}, T_{in}) of inlet thermodynamic conditions. As shown in Fig. 7.9a, b, TSI associated to the uncertainty on p_{in} vary from 8 to 44 % while vary from 39 to 83 % for uncertainty on T_{in}. For the uncertainties on two geometrical parameters, θ and ϕ (see Fig. 7.9c, d), TSI vary from 7 to 25 % and from 0.7 to 2.9 %, respectively. TSI associated to the uncertainties on thermodynamic model, i.e. ω, $c_{v\infty}$ and n, and on the geometrical parameter ϕ, are less than 0.29 %, then they are negligible with respect to the TSI criterion.

For each design of the DOE that has been previously computed for kriging metamodel, the reduced stochastic problem is performed and the statistics are computed in terms of mean and standard deviation for PO.

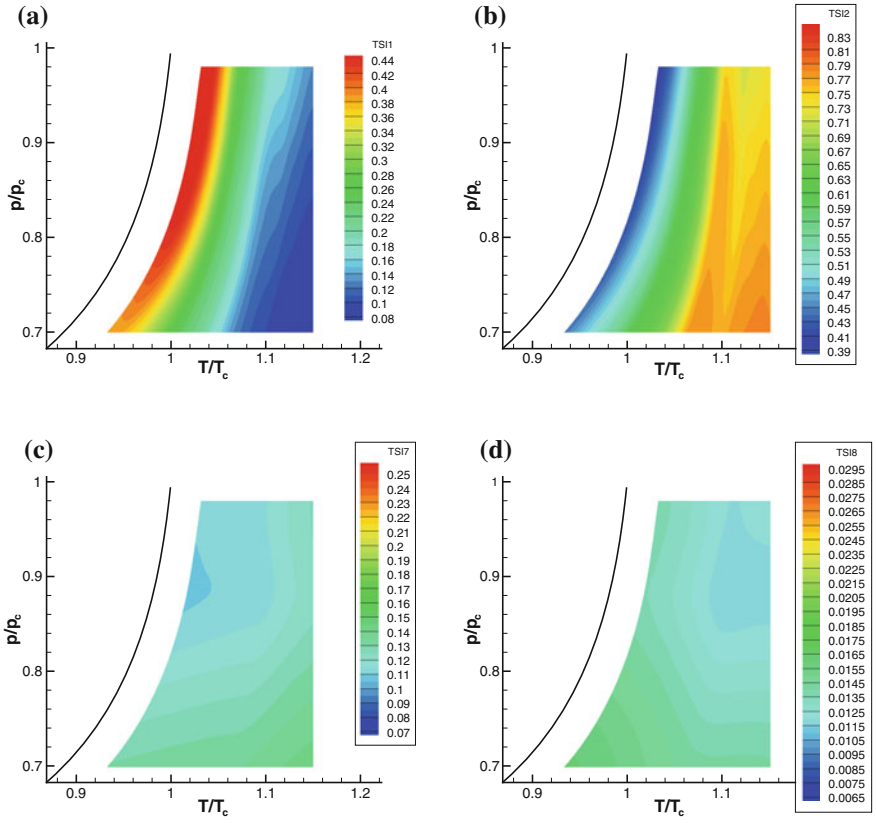

Fig. 7.9 TSI contours in the plan p-T for each uncertainty. **a** p_{in}. **b** T_{in}. **c** θ. **d** ϕ

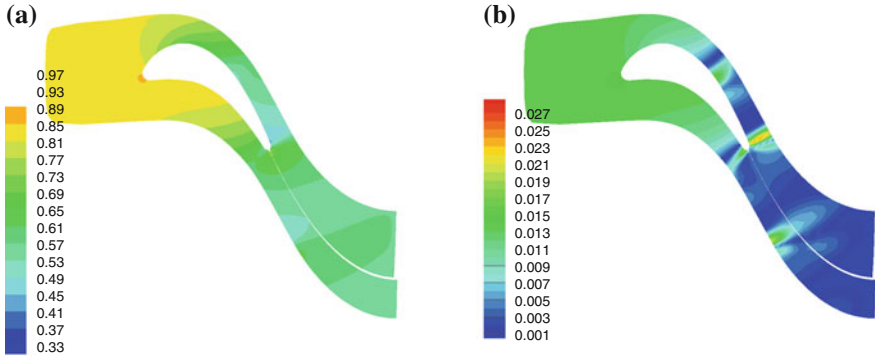

Fig. 7.10 Mean (**a**) and standard deviation (**b**) for pressure for some optimal individuals

Then, twenty individuals evolved during forty generations. The converged Pareto front is represented in Fig. 7.4. Various configurations are obtained with a large variation of the PO, going from 0.91 to 1.46.

The proposed method, in terms of criterion for reduction problem, has been compared with the one proposed in [4]. In particular, the Pareto front is different with the exclusion of several profiles. This is due to a lack of accuracy when only variance is considered in the reduction strategy. With respect to the old version, the introduction of a more strict criterion (based on kurtosis) increases the global computational cost, even if with a greater accuracy.

In Fig. 7.10, the mean pressure is shown in the computational domain. Generally, high inlet turbine pressures are associated to high mean of PO, displaying a strong dependence of turbine performances from thermodynamic inlet conditions. In a similar way, standard deviation of the pressure is reported in Fig. 7.10. Variance is concentrated around the compression shock location near the trailing edge.

7.5 Conclusions

In this work, the interest of using high-order decomposition for reducing the number of uncertainties in a robust optimization problem is assessed. In particular, sensitivity of different problems with respect to the variance or kurtosis decomposition is illustrated. Finally, a well-known optimization algorithm is modified for including this adding information in the reduction loop.

References

1. Xiu D, Karniadakis GE (2002) The Wiener-Askey polynomial Chaos for stochastic differential equations. SIAM J Sci Comput 24(2):619–644. doi:10.1137/S1064827501387826
2. Foo J, Karniadakis GE (2010) Multi-element probabilistic collocation method in high dimensions. J Comput Phys 229:1536–1557. doi:10.1016/j.jcp.2009.10.043, http://linkinghub.elsevier.com/retrieve/pii/S0021999109006044

3. Eldred MS, Webster, Constantine PG (2008) Design under uncertainty employing stochastic expansion methods. In: Paper 20086001. AIAA
4. Congedo P, Geraci G, Abgrall R, Pediroda V, Parussini L (2013) Tsi metamodels-based multi-objective robust optimization. Eng Comput (Swansea, Wales) 30(8):1032–1053
5. Abgrall R, Congedo P, Geraci G, Iaccarino G (2012) Decomposition of high-order statistics. INRIA Research Report (RR-8193), pp 1–40
6. Sobol I (2001) Global sensitivity indices for nonlinear mathematical models and their Monte Carlo estimates. Math Comput Simul 55(1–3):271–280. doi:10.1016/S0378-4754(00)00270-6, http://linkinghub.elsevier.com/retrieve/pii/S0378475400002706
7. Gao Z, Hesthaven JS (2010) Efficient solution of ordinary differential equations with high-dimensional parametrized uncertainty. Commun Comput Phys 10(2):253–278
8. Deb K, Pratap A, Agarwal S, Meyarivan T (2002) A fast and elitist multiobjective genetic algorithm: NSGA-II. IEEE Trans Evol Comput 2(6):619–644
9. Abgrall R, Congedo PM, Santis DD, Razaaly N (2014) A non-linear residual distribution scheme for real-gas computations. Comput Fluids 102:148–169. doi:10.1016/j.compfluid.2014.06.031
10. Congedo P, Corre C, Cinnella P (2011) Numerical investigation of dense-gas effects in turbomachinery. Comput Fluids 49:290–301
11. Cinnella P, Congedo PM, Pediroda V, Parussini L (2011) Sensitivity analysis of dense gas flow simulations to thermodynamic uncertainties. Phys Fluids 23, 116, 101:1–20